Title
Velocity and Scalar Characteristics of Premixed Turbulent Flames Stabilized by Weak Swirl

Author
Cheng, R.K.

Publication Date
1994-07-01

LBL-36000
UC-400
Preprint

Lawrence Berkeley Laboratory
UNIVERSITY OF CALIFORNIA

ENERGY & ENVIRONMENT DIVISION

Submitted to Combustion and Flame

Velocity and Scalar Characteristics of Premixed Turbulent Flames Stabilized by Weak Swirl

R.K. Cheng

July 1994

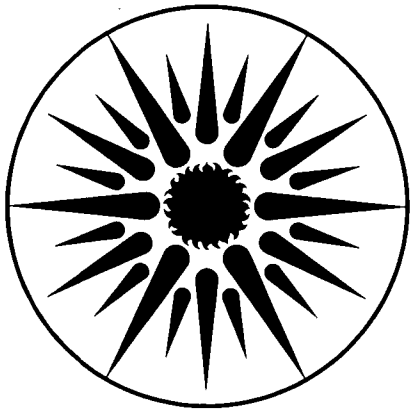

ENERGY & ENVIRONMENT DIVISION

Prepared for the U.S. Department of Energy under Contract Number DE-AC03-76SF00098

DISCLAIMER

LBL-36000
UC-400

Velocity and Scalar Characteristics of Premixed Turbulent Flames Stabilized by Weak Swirl

R. K. Cheng

Combustion Group
Energy & Environment Division
Lawrence Berkeley Laboratory
Berkeley, CA 94720

July 1994

This work was supported by the Director, Office of Energy Research, Office of Basic Energy Sciences, Chemical Sciences Division of the U.S. Department of Energy under Contract No. DE-AC03-76F00098.

Velocity and Scalar Characteristics of Premixed Turbulent Flames Stabilized by Weak Swirl

R. K. Cheng

Combustion Group
Energy & Environment Division
Lawrence Berkeley Laboratory
Berkeley, CA 94720

Abstract

Velocity and scalar statistics of premixed flames stabilized in a novel weak-swirl burner have been studied under a broad range of mixture and turbulence conditions. The non-reacting flows are also investigated to determine the influence of weak-swirl on isotropic turbulence. Deduced from the data are the flame speeds, combustion induced flow acceleration, flame generated turbulence, and flame crossing frequencies. They are compared with previous results obtained in other flame configurations. Three series of experiments are conducted to investigate the evolution of velocity statistics with decreasing equivalence ratios. Under very lean conditions ($\phi = 0.6$) , the velocity profiles have no characteristic features and are not very different from the corresponding non-reacting profiles. An indicator parameter, K_T , derived from fundamental mixture and flow properties is developed to estimate the relative influences of the turbulence stretch and the mean aerodynamic stretch on combustion induced flow acceleration. The analysis shows that intense turbulence and bulk stretch (i.e. large values of K_T) can obscure and counteract the dynamic effects of combustion.

Introduction

Recently, we reported the development of a novel weak-swirl burner for laboratory studies of premixed turbulent flames [1]. This burner stabilizes open freely propagating yet steady premixed flames that are free of flow or physical constraints. The flame zone levitates above the burner exit. It is adiabatic and is easily assessable by laser diagnostics for detail interrogation. The burner design is relatively simple, consists of a cylindrical swirler section attached to a concentric nozzle and a settling chamber (Figure 1). This flow supply apparatus has been used previously for many of our flame configurations [2-4]. Weak-swirl is produced by two tangential air injectors fitted to the rim of the swirler section. Typical swirl intensities needed for flame stabilization are very low. The swirl number, S, determined based on the definition Beer and Chigier [5] is between 0.05 and 0.3. Conventional swirl burners operate at $S >> 1$.

Our first paper [1] was focus on determining the basic flame stabilization mechanism and some overall flame behavior. We reported velocity and scalar measurements made in six reacting and non-reacting cases all having the same total flow rate. Both turbulent and non-turbulent flames were studied (i.e., with or without the use of a turbulence generating grid). The study showed that flame stabilization by weak-swirl does not involve flow recirculation as in most other methods, e.g. strong swirl [6,7] and stabilizers [2,4]. Instead, weak swirl generates a divergent flow region above the burner where the mean axial velocity decreases almost linearly. This provides a very stable configuration for the flame to maintain itself at the position where the local mass flux equals the burning rate. The stabilization mechanism is similar to that of stagnation flow stabilized flames. Flow stagnating against a plate [3] or in opposing streams [8] are two configurations developed for premixed turbulent flame studies. The stagnation flow configurations are constrained because the flow velocity reduces to zero downstream of the flame zone. Under certain conditions, the close proximity of the stagnation point to the flame can introduce complexity leading to flame extinction. Flames stabilized by weak-swirl, on the other hand, are free of these influences.

The most interesting and significant flame feature we have found is that the flame zone is free of the influence of swirl. Measurements of the circumferential velocity component, w, show that the swirling motions occur only in the outer region near the burner rim. Towards the center of the burner, no swirling motion is found. Consequently the flame is free of the influence of shear. The flowline trajectories through the flame zone show that these flames are, in essence, slightly stretched planar premixed turbulent flames. Their mean aerodynamic stretch rates, a_b, are about an order of magnitude lower than those of stagnation flow flames

[3]. Theoretically, the flowfield can be treated as a flame stabilized within a stagnation flow with the stagnation point far downstream from the flame zone. This flame configuration is therefore a close approximations of the normal one-dimensional planar flame and stretched premixed turbulent flames of the Bray-Moss-Libby model [9].

The operating range of the weak-swirl burner is much wider than any laboratory burners [2-4, 8,10]. This can be attributed to the fact that flame blow-off and flash-back are effectively prevented because the flow velocity upstream of the flame zone is higher than the flame speed and the flow velocity downstream is lower. Consequently, this burner configuration would be suitable for investigating many near limit turbulent flame phenomena such as local flame extinction, very lean premixed turbulent flames, and intense turbulent flames (i.e. flames approaching the so-called distributed reaction zone). These flame phenomena are not very well understood because of the difficulties in maintaining a sufficiently steady flame for detailed interrogation. We have already built and successfully tested a smaller weak-swirl burner that supports stable flame propagation under intense turbulence ($u' > 1.5$ m/s) [11].

The lean methane/air limit of $\phi = 0.57$ found for this burner is close to the laminar flammability limit. Under these very lean conditions, the emission of oxides of nitrogen (NO_X) is greatly reduced. The NO concentrations measured in our burner for $\phi = 0.6$ and 0.7 are respectively 4 and 7.5 PPM. These concentrations are identical to those measured in laminar flat flame burners. The power output of the laboratory burner (about 30 KW) is the same as typical home furnaces or small commercial water heaters. Therefore, the weak-swirl burner can also be exploited for developing low emission practical applications.

Given the practical and fundamental significance of the weak-swirl burner, further investigation of flame and flow characteristics is important to provide the foundation for future scientific and technological research. The objective of this paper is to present a more complete characterization of the scalar and velocity statistics of weak-swirl stabilized premixed flames. The evolution of the turbulence in the non-reacting flow is also determined as there has been very few reports in the literature regarding the influence of swirl on isotropic turbulence. The flame experiments include turbulent and non-turbulent cases at different flow rates. Three series of experiments are also carried-out to infer, for the first time, changes in the velocity statistics with equivalence ratios from very lean (CH_4 $\phi = 0.6$, C_2H_4 $\phi = 0.5$) to stoichiometric. Such a study would not be possible in other flame configurations due to flash-back and blow-off (see Table I, Reference [2]). The experiment measurements consist of conditional velocities and flame crossing statistics. These data are analyzed the same way as our previous work [2].

Apparatus, Diagnostics, Data Reduction, and Experimental Conditions

Details of the burner and laser diagnostics are described previously [1], a brief summary is included here. Figure 1 shows a schematic of the burner. The only change made to the burner is to increase the number of air injectors from two to four. Each jet can be adjusted independently to produce a uniform divergent flowfield. With the use of four injectors, flame zone symmetry is generally improved. However, slight flame asymmetry is unavoidable under some conditions.

Flow velocities are measured by a two-component four beam LDA system consisting of two TSI frequency counters. All four beams are frequency shifted to remove directional ambiguity. The differential shifting frequency for both components is 3 MHz. The LDA system is arranged to measure the axial velocity component, U, (two 488 nm beams) and the radial component, V (two 514 nm beams). As shown previously, the circumferential component, W, is effectively zero in the vicinity of the flame, this component is therefore not measured here. Seeding the fuel/air flow with Al_2O_3 particles or silicone oil aerosol measures respectively unconditioned and conditioned (reactants) velocities. Mean velocities, RMS velocities, and Reynolds stresses are deduced from 2048 or 4086 validated velocity pairs obtained using a 10 μs coincidence criterion. Analysis of the conditional and unconditional velocity statistics is carried-out as described in Reference [2]. The velocity spectra for the longitudinal velocity fluctuations, u', are measured by sampling the analog counter output at a fixed rate of 10 KHz. The spectral measurements are made only when the data rate exceeds 12 KHz. As discussed in reference [12], this is a very convenient means to obtain flame spectra.

The flame crossing frequencies, ν and reaction progress variable, $\overline{c}$, are measured by the Mie scattering from oil aerosol (MSOD) method [13]. This is a convenient method to measure time and length scales of premixed turbulent flames. The optics is relatively simple and our system uses the 488 nm beams produced by the LDA transmitting optics. This enables us to switch conveniently between LDA and Mie scattering measurements. Mie scattering intensities at the beam waist is collected by a photomultiplier tube arranged perpendicularly to the beam direction. As the oil aerosol burns and evaporates at the flame zone, the output Mie signal resembles that of a telegraph. This signal is processed on-line using a two threshold criterion. The mean transit times for the reactants and products periods are used to compute ν and $\overline{c}$.

The experimental conditions are listed in Table I. They include four flames from our previous work (SWF1 - SWF4) and seventeen new flames (SWF5 - SWF21) obtained under lower flow rate (U_∞ = 3.0 m/s compare to 5.0 m/s)*. The experiments include methane/air and ethylene/air flames with or without incident turbulence. Turbulence is generated either by a square grid of 5 mm spacing or by a perforated plate with 3.2 mm holes. All the flame conditions are within the so-called wrinkled laminar flame or flamelet regime. As reported before, the swirl numbers, S, for SWF1 to SWF4 are about 0.07 to 0.08 [1]. For SWF5 to SWF21, S are about 0.05 to 0.06. The small change in swirl number for a difference in flow rate of 60% suggests that the swirl number for flame stabilization may be independent of the flow rate. Flame stabilization is also possible at higher and lower flow rates (up to U_∞ = 7.0 m/s and down to 1.0 m/s). Under the lowest flow rate, the flame is not much larger than the 50 mm diameter of the fuel/air core.

Results

Incident turbulence and flowfields

Figure 2 shows direct flame luminosity photographs of a non-turbulent flame and a turbulent flame. The photographs were captured by a video camera with shutter speed of 1/4000 sec to freeze the flame motions. As reported previously and shown more clearly here in Fig. 2(a), flames without incident turbulence are not perfectly planar. They have rather large flame wrinkles, therefore, we call them non-turbulent flames to distinguish them from planar laminar flames found in flat-flame burners. The differences in the sizes and shapes of the non-turbulent and turbulent flame wrinkles are shown quite clearly on Figures 2(a) and 2(b). The video also shows that both the non-turbulent and turbulent flames exhibit flame bouncing i.e. gross up and down movement of the entire flame brush. The flame bouncing motion is similar to that observed in flames stabilized in opposing streams [8].

Flame bouncing may be explained by the turbulence characteristics shown on the streamwise velocity fluctuation spectra (Figure 3). These u' spectra are measured at 10 mm above the burner exit for a grid generated turbulent flow of U_∞ = 3 m/s. The three conditions are (1) isothermal flow without swirl, (2) isothermal flow with swirl, and (3) in the reactants of SWF19. The non-swirling turbulence spectra is typical of grid generated turbulence shown in our earlier

---

* U_∞ is the mean velocity at the burner exit without swirl. It is used here as an indication of the total flow rate. The introduction of swirl lowers this exit velocity.

work. The introduction of swirl reduces the local flow velocity from 3.0 m/s to about 1.0 m/s, but increases the RMS velocity slightly from 0.174 m/s to 0.194 m/s. The increase in spectral energy appears mostly in the low frequency below 100 Hz. The spectra for the reacting case is almost identical to the non-reacting case with swirl. These low frequency contributions in both reacting and non-reacting swirl flows suggest large scale fluctuations. The integral length scales deduced for the spectra are 1.07 mm for the non-reacting flow with no swirl , 1.67 mm for the non-reacting swirl flow and 2.02 mm for SWF19. These values are small compared to the flame wrinkle sizes shown in Figure 1(b).

The source of the low frequency fluctuation is difficult to determine precisely. The near zero Reynolds stress measured at the burner center demonstrate that shear is not the production mechanism. Turbulence production by mean aerodynamic stretch may be a possible cause. In stagnation flows, turbulence ceases to decay because of mean aerodynamic stretch[3]. But the stretch rates in our flows are an order of magnitude lower than in stagnation flows, and do not seem likely to produce the level of turbulence increase observed here. The most plausible explanation for the increase in low frequency fluctuations seems to be the instabilities generated by the interaction between the four swirl jets and the mean flow. These instabilities may also explain the wrinkles shown for the non-turbulent flames. Flucautaions in the radial pressure gradients assocated with the flow instabilities can augment Rayleigh instabiliy of the flame front. The important issues, however, is that these flow instabilities produces gross flame bouncing and wrinkling of the flame seems a secondary effect. Therefore, some allowance has to be made when comparing the integral length scales of the incident turbulence with flame wrinkle scales.

The velocity vectors plotted in figure 4 (a) through (d) show the overall features of the reacting and non-reacting flowfields. In Figure 4(a) for the non-reacting flow of SWF10, the divergence region produced by weak-swirl is quite evident. The mean velocity decreases with increasing x and reduces to almost zero at x = 55 mm. The vectors also show the uniformity of the flow velocity at different heights above the exit. Flow reversal or flow recirculation is not observed. The corresponding velocity vectors of SWF10 (Figure 4(b)) show that the flame changes only the flow in the products zone. Below the leading edge of the flame zone the flow vectors are almost identical to those of Figure 4(a). The flame leading edge contour is slightly concave towards the reactants. This is a consistent feature of all the non-turbulent flames (see Figure 2(a)). Along the centerline, all the velocity vectors are vertical, and parallel. The flow is essentially non-divergent, therefore, this flame configuration produces one of the closest approximation to 1-D flames.

The use of the turbulence generator creates some changes in the overall flow pattern of the non-reacting flow. Compared to Figure 4(a), the flowfield shown in Figure 4(c) is not uniform across the burner but is characterized by a small velocity deficit at the center. This deficit becomes pronounced at x = 25 mm and persists downstream. The fact that this velocity deficit is found only in turbulent flows suggests its cause to be associated with radial transport of turbulent momentum. Despite the deficit, the non-reacting turbulent flow remains non-recirculatory. The velocity deficit also explains the convex turbulent flame shape. The leading edge of SWF18 (Figure 4(d)) shows that the flame is slightly off-centered even though the flow vectors upstream of the flame leading edge are symmetrical. The extend of flame asymmetry for SWF18 is the maximum we have observed. For example, the flowlines of SWF4 shown previously [1] is more symmetric. Due to flame asymmetry, the flow distribution downstream of the flame zone is non-uniform. Local surge in velocity is shown near x = 25 mm, r = 10 mm. However, the flow in the products remains relatively non-divergent throughout.

Correlation of flame speed

As shown by the velocity vectors, the flow at the center is normal to the flame brush. In accordance with the definition developed for stagnation flow stabilized flames, the velocity at the flame leading edge ($\bar{c} \approx 0.05$) can be considered as the flame speed, S_f. For flames with slight asymmetry (e.g. SWF18) the uncertainly introduced by the use of the centerline velocity is found to be relatively small. This is because unlike other flame configurations such as v-flames, the angle formed between the velocity vectors and the flame orientation are close to normal. Small variations in this angle does not results in large changes in the flame speed. Listed in Table I and shown in Figure 5 are the results deduced for all our flames. The flame speed normalized by the laminar flame speed, S_L are correlated with the normalized averaged RMS velocity, q'/S_L. Also shown are the results obtained for stagnation plate stabilized flames. The stagnation flames are listed in Table II. As can be seen, S_f/S_L deduced for the weak-swirl stabilized flames increase linearly with q'/S_L and are also in accord with the stagnation flame results. Note that the range of the weak-swirl flames extends to much higher range of q'/S_L. With the use of other turbulence generators, it is possible to extend this domain to even higher values of q'/S_L so to investigate flame conditions within the corrugated flame and distributed reaction zone regimes [11].

Mean profiles

The mean centerline scalar profiles $\bar{c}$ and ν, unconditioned and conditioned mean and RMS velocities : U, u', v', U_r, u'_r, v'_r, U_p, u'_p and v'_p for SWF4 are shown in Figures 6 (a) - (d). Using the procedure described previously [2], the conditioned mean and RMS velocities for the products, U_p and u'_p ,v'_p are deduced by deconvolving the joint probability density functions (jpdf) of the conditioned reactant velocity fluctuations from that of the unconditioned velocity fluctuations.

The scalar profiles of Figure 6(a) are typical of wrinkled laminar flames found in other flame configuration such as stagnation flow stabilized flames, v-flames and large conical flames [2]. The main differences are the flame zone thickness and the maximum flame crossing frequency ν_{max}. A flame thickness of 20 mm for SWF4 at the centerline is typical of all the turbulent conditions we have investigated. This is comparable to the stagnation flow stabilized flame thicknesses. The flame thicknesses determined for the non-turbulent flames are about 10 mm. It is large compared to the laminar flame thickness of about 1 mm. This seems to be caused by a combination of flame bouncing and slight flame wrinkling.

The flame crossing frequencies, ν, of the turbulent flames, typically between 60 Hz and 120 Hz are close to those measured in stagnation flow stabilized flames. The values of ν for v-flames and piloted conical flames can reach up to 1000 Hz. The reason for the order of magnitude difference is that ν is related to the convection velocity of the flame wrinkles. In the oblique v-flames and conical flames, flame wrinkles are convected along the flame brush close to the free stream velocity (about 5 to 7 m/s).

Representative distributions of ν as functions of $\bar{c}$ are compared in Figure 7. The $n(\bar{c})$ profiles are nbormalized by the integral $\int_0^1 \nu(\bar{c})d\bar{c}$ to compare the shape of the distributions with the symmetrical theoretical distribution of the Bray-Moss-Libby (BML) model [9]. Self-similarity shown by the experimental results is apparent but they are all skewed towards $\bar{c} > 0.5$. In fact, this skewness is the only consistent feature of all the premixed turbulent flames we have studied, as mentioned previously [14], is probably associated with the formation of flame cusps. It is of interest to note that the profile of the non-turbulent flame (SWF1) also has the same distribution. This may be an indication that ν is not very sensitive to the differences in flame wrinkle topology. The maximum ν found for SWF1 is only 26 Hz. This supports the notion that for the non-turbulent flame, the major contribution of ν is due to flame bouncing. As shown in Figure 3 the increase in spectral energy with swirl occur near this frequency range.

Returning to Figure 6(b) the unconditioned axial velocities, U, profile shows a gradual decrease in the reactants ($x < 20$ mm) followed by an acceleration in the flame zone (20 mm $< x <$ 46 mm). The velocity in the products zone ($x > 46$ mm) remains constant, and this is the main difference between these profiles and those of stagnation flow stabilized flames. Within the flame zone, the two conditioned mean velocities profiles U_r and U_p show a relative velocity, $\Delta U = U_p - U_r$, of approximately 1.8 m/s. This relative velocity is the main contributor to turbulent transport of scalar and momentum. The sign of ΔU suggests turbulence transport in the counter-gradient sense. These are the characteristic features of wrinkled laminar flames.

The relative velocity, ΔU, is usually not constant within the flame brush. It is sensitive to changes in turbulence intensity, flow divergence and conditions downstream. A convenient means to normalize ΔU is by the relative velocity of a normal 1-D laminar flame $\Delta u_L = S_L (\tau -1)$ where τ is the density ratio ρ_r/ρ_p. Δu_L is a fundamental property of each flame representing its potential to induced flow acceleration. The normalized $\Delta U/\Delta u_L$ profiles for a number of flames are compared in Figure 8. The most interesting results is shown by the non-turbulent flame SWF1 where $\Delta U/\Delta u_L$ remains at unity within the flame brush. The profile of another non-turbulent flame SWF5 is somewhat lower, starting at $\Delta U/\Delta u_L = 0.8$ then decreasing to about 0.6. The two non-turbulent flame profiles demonstrate that aside from flame bouncing, the overall behavior of the non-turbulent flames are consistent with that of laminar flames. The values of $\Delta U/\Delta u_L$ for the turbulent flames are all grouped around 0.6 for $\bar{c} < 0.5$ but are more scattered for $\bar{c} > 0.5$. The scatter is most likely caused by the difference in downstream conditions. Compared to similar measurements made in other configurations (Figure 8, Reference [2]), the results show here are higher than those of the stagnation flames and conical flames but less than those of v-flames. Both stagnation flames and conical flames have significant flow divergence in the products. The v-flames, however, are characterized by flow convergence in the product zone.

Returning again to Figures 6 (c) and (d), the RMS velocity profiles show typical wrinkled laminar flames features. A peak in the u' profiles is the predominant feature. This peak value tends to scale with the relative velocity ΔU. The $u'_{max} = 1$ m/s peak of SWF4 ($\Delta U = 1.8$ m/s) is modest compared to the $u'_{max} = 2.75$ m/s measured in S9 of Table II ($\Delta U = 3.8$ m/s). The true magnitude of flame generated turbulence is represented by the difference in u'_p and u'_r. Because ΔU contributions to unconditioned velocity fluctuations are mainly in the direction normal to the flame brush, the v' profile has a only a very small peak which is not much higher than v'_p. Turbulence downstream in the products zone becomes slightly anisotropic with $u' > v'$. This anisotropy is also found in stagnation flames.

To show the uniformity of the flame brush, the centerline profiles are compared with the off-center profiles obtained along off-center flowlines. Shown in Figure 9 and 10 are, respectively, the magnitude of the 2-D velocity vector |U| and q' for SWF1 and SWF4. The flowline trajectories of the two flames are shown in Figure 6 of Reference [1]. From Figure 9, it is clear that the non-turbulent flame is quite uniform. There is very little difference between the two sets of |U| and q' profiles. This is not the case for SWF4, there are noticeable differences upstream and downstream of the flame zone. This is directly related to the non-uniformity of the flowfield as shown Figure 4(d). However, these differences are mild compare to those observed in stagnation flames (Figure 7 Reference [2]).

Changes in flame characteristics with ϕ

The wide range of operating range of the weak-swirl burner allows a systematic investigation of the changes in the velocity statistics from strong burning near stoichiometric flames to weak burning lean flames. The three experimental series conducted are SWF6 - SWF9 for C_2H_4/air with plate turbulence ($0.75 < \phi < 0.5$), SWF12 -SWF16 for CH_4/air flames with plate turbulence ($1.0 < \phi < 0.6$) and SWF17-SWF21 with grid turbulence ($1.0 < \phi < 0.6$). The centerline profiles of SWF12-16 are shown in Figure 11. Also shown is the profile of a lean ($\phi = 0.6$) non-turbulent flame (SWF11). As noted previously, the leanest CH_4/air that can be stabilized in v-flame and piloted conical flame configurations are only about $\phi = 0.7$. The leanest stagnation flames are around $\phi = 0.75$.

Figure 11(a) show the evolution of the mean axial velocity profiles with ϕ. The stoichiometric flame (SWF12) shows the characteristic increase in mean velocity due to the flame (Figure 6(a)). This increase becomes weaker with decreasing ϕ and is not present on the profiles of the leanest flame (SWF16). The corresponding non-turbulent flame profile (SWF11) is also relative flat and the slight increase actually occurs in the product zone ($x > 22$ mm) downstream of the flame. The changes in these profiles are consistent with Δu_L decreasing from 2.72 m/s at $\phi = 1$ to 0.73 m/s at $\phi = 0.6$. Due to the their low value of Δu_L the profiles of the weak burning flame SWF16 lack any significant features. Of course, there are other flow and flame geometry factors which influence whether or not flow acceleration occurs within the flame zone. As concluded in a comparison of stoichiometric CH_4/air flame generated in three different burner [2], mean flame stretch is also a major influence. Under high stretch (about 450 $sec.^{-1}$) flow acceleration is absent even for near a stoichiometric flame [8]. Because all of our flames have the same low stretch rates (about 25 to 30 $sec.^{-1}$), weakening of Δu_L seems the only cause of the changes shown here.

Similar trends are also shown for the profiles of q' (Figure 11 (b)). Maximum value of q' of each flame decreases with decreasing ϕ. For SWF16, the q' profile is again flat. The corresponding SWF11 profile show increase in q'. Again, these increases occur in the products region downstream from the flame zone. The lack of any significant features on both U and q' profiles of SWF16 indicates that it would be very difficult to interpret the velocity data without the support of additional scalar information.

The jpdfs of the velocity fluctuations further illustrate the drastic changes in velocity statistics with ϕ. The contour maps of the jpdf at the position of maximum q' (at about $\bar{c} = 0.5$) are compared in Figure 12. For the stoichiometric flame SWF12, the jpdf is bi-modal. These contours, however, do not form two distinct islands as in SWF4 (Figure 5, Reference [1]). This is due to the higher turbulence intensities of SWF12 . Higher turbulence intensity means that the contours covers a larger area on the u'-v' plane resulting in merging of the lower contours. The two peaks of SWF12 are aligned on the v' = 0 axis indicating that the flame zone is normal to the x axis. The separation between the to peaks is ΔU and the u'=0 axis essentially separates the contributions from the reactants (u'<0) and the products (u'> 0). The higher turbulence intensities in the products is represented by the large spread of the contours in the upper half of the u'-v' plane. With decreasing ϕ (SWF13 to SWF15), the bi-modality of the jpdf is less and less distinct with the two peaks merging together. This is due primarily to the decrease in ΔU (which scales with Δu_L). As ΔU reduces even further, the two peaks are completely merged (SWF16). The jpdf of SWF16 is not very different than the jpdf of the incident turbulent. The incident u' of 0.34 m/s is the same order as Δu_L which is only 0.72 m/s. Because $\Delta U/\Delta u_L$ is typically 0.5 to 0.6 , the turbulence fluctuations in SWF16 can easily overwhelm the effects of flow acceleration. This is why the |U| and q' profile of SWF16 is featureless. For the non-turbulent lean flame (SWF11), the two peaks are present but difficult to discern. They are separated by only 0.5 m/s and it is not possible to deconvolve the conditioned velocities with high degree of accuracy. The spreading of the contour lines in the v' direction also explains the increase in the q' shown in Figure 11(b).

Discussion

The changes in the velocity profiles with ϕ indicate a coupling between the effects of combustion induced flow acceleration, flow divergence and turbulence intensity. Depending on the relative significance of these effects, the flame can cause significant changes in the velocity statistics or none at all. To gain a better insight on their influences, we use an indicator parameter K_t which compares the source of acceleration, Δu_L with the two sinks: turbulence stretch, a_T, ($a_T = u'/l_x$, l_x is the integral length scale) and the mean aerodynamic

stretch, a_b. Δu_L, a_T, and a_b are respectively properties of the mixture, incident turbulence and flow or flame geometry.

$$K_T = (a_T + a_b) / \Delta u_L \qquad (1)$$

K_T takes the form of an extinction criterion, $K_E = 2a_b/ \Delta u_L$, developed for flames stabilized in opposing streams [8]. It has a unit of inverse length, which is the same as, Σ, the flame area per unit volume, used for predicting the turbulent burning rate [14].

The effect of turbulent stretch on turbulent flame statistics can be interpreted in terms of a kinematic model proposed by Cheng et. al. [15]. The flamelets generate flow acceleration in a direction normal to the local flame orientation. As turbulence intensity increases, the flamelets are more wrinkled. Consequently. the directions of the flow vectors generated normal to the flamelets become more random. This can result in an increase of the turbulence fluctuations in the products and a net reduction in ΔU. Bulk stretch generates either flow divergence or convergence depending on its sign. Most laboratory flames have divergent flowfields and the overall effect, again, is to reduce ΔU.

Figure 13 compares the value of K_T obtained for several weak-swirl stabilized flames, two stagnation plated stabilized flames and the flame stabilized in opposing streams reported in Kostiuk et. al. [8]. As discussed earlier, the reacting and the non-reacting flowfields of the opposing flame of Kostiuk et. al. are almost identical. This flame has the highest value of K_t. For the series SWF12 to SWF16, K_T increases from 50 to about 130 showing that flames with large values of K_t produce very little change in the flowfield. As for flames with low values K_T such as SWF4, SWF11, SWF12, and S9, flow acceleration is clearly shown. The analysis also suggests that the effects of turbulence stretch and mean aerodynamic stretch are additive. For example, SWF14 and the flame of Kostiuk et. al. experience the same level of turbulence stretch. But the larger mean aerodynamic stretch in the opposing flow is responsible for the differences in the behavior of the two flames. The implication is that the criterion for flame phenomenon such as extinction should include both stretch effects. Note that K_T should also apply to flames with convergence flowfield. With a_b being negative, the effect of mean aerodynamic stretch would counteracts that of turbulence stretch and reduces K_T. This agrees with the physical notion that flow convergence will enhance flow acceleration and thus increase ΔU. Since most flame flowfields are divergent, this may not be easy to validate experimentally.

The concept of an indicator, K_T, for estimating the effects of premixed turbulent flame on the velocity statistic, though qualitative, is an attempt to reconcile the results from many different experimental flame configurations. At present, theoretical prediction of the flowfield generated by premixed turbulent flames still relies on empirical input to achieve closure. A more formal theoretical development of a such parameter involving only the fundamental mixture and flow properties would be very helpful to theoretical development.

Conclusion

Our experimental study demonstrates that the weak-swirl burner is a simple and versatile laboratory flame configuration for fundamental studies of premixed turbulent combustion. The flames are adiabatic, locally normal to the approach flow, experience low mean aerodynamic stretch, and are very accessible to diagnostics. Its large range of operating conditions enables the mixture and turbulence conditions to be varied systematic. The work reported here covers three series of experiments to investigate changes in the flame flowfield with equivalence ratio.

Measurements of the turbulence spectra in the non-reacting flow shows that weak-swirl induces low frequency fluctuations which cause gross flame brush bouncing. While the non-turbulent flow is uniform, the turbulent flow has a small velocity deficit centered on the burner axis. This explains the difference in the convex and concave shapes of the turbulent and non-turbulent flames.

The turbulent flame speeds deduced for twenty-one flames show linear dependence on averaged RMS velocity. These results cover a much wider range of conditions than those reported previously for stagnation flow stabilized flames. The scalar and conditioned velocity statistics show that flame behavior is typical of premixed turbulent flames within the flamelets or wrinkled laminar flame regime. The existence of a relative velocity ΔU, local peaks in the unconditioned velocity fluctuations profiles and flame generated turbulence in the products are found for most flames. Comparison of the profiles at different off-center flowline trajectories shows that the flame brushes are more uniform than other laboratory flames.

Significant changes are found in the velocity profiles when the equivalence ratio is lowered. Under the leanest condition ($\phi = 0.6$), the profiles have no characteristics features and are not very different than the non-reacting profiles. These changes are attributed to a weakening of the lean flames' ability to generate significant flow acceleration and to the turbulence intensity which can obscure these relatively small effects. A parameter, K_T, which compares the effects of combustion induced flow acceleration, turbulence stretch and mean aerodynamic stretch is

developed. It shows that flames with high values of K_T have very little effect on the velocity field. Significant changes in the velocity statistics are found only for flames with low values of K_T. The analysis also supports the notion that the effects of turbulence stretch and mean aerodynamic stretch are additive. This may have implication on future work on the conditions leading to flame extinction.

Nomanclature

Flow Parameters

U, u'	mean and RMS axial velocities
V, v'	mean and RMS radial velocities
W, w'	mean and RMS circumferential velocities
$\overline{u'v'}, \overline{u'w'}, \overline{v'w'}$	Reynolds stresses
$\|U\|$	magnitude of 2D velocity vector $\equiv \sqrt{U^2+V^2}$
q'	average RMS velocity $\equiv \frac{1}{2}\sqrt{u'^2+v'^2}$
l_x	integral length scale
a_b	mean aerodynamic stretch = dU/dx
a_T	turbulent stretch $\equiv u'/l_x$
S	swirl number = $\frac{\pi r_0 R}{A_t}\left(\frac{m_\theta}{m_\theta + m_A}\right)$; r_0, radius of the swirl jets; R, burner radius; A_t, total area swirl air jets; m_θ tangential mass flow rate; m_A axial mass flow rates.

Flame Parameters

ϕ	equivalence ratio
ρ	density
τ	density ratio = ρ_r/ρ_p
$\bar{c}$	progress variable = $(\bar{\rho}-\rho_p)/(\rho_r-\rho_p)$
S_L	laminar flame speed
S_F	flame speed of turbulent and non-turbulent flames
ΔU	relative velocity $\equiv U_p - U_r$
Δu_L	relative velocity of a normal 1-D laminar flame = $S_l(\tau - 1)$
Σ	flame area per unit volume
ν	flame crossing frequency
K_t	indicator parameter for the effects of flames on turbulence, $(a_t + a_b)/\Delta u_L$

K_F	extinction criterion = $2a_b / \Delta u_L$
Subscripts	
L	laminar condition
T	turbulent condition
p	conditioned products properties
r	conditioned reactants properties
∞	free stream conditions without swirl

Acknowledgment

This work was supported by the Director, Office of Energy Research, Office of Basic Energy Sciences, Chemical Sciences Division of the U. S. Department of Energy under Contract No. DE-AC-03-76SF00098. The authors would like to thank Dr. Ian G. Shepherd for the valuable discussion and to acknowledge Mr. Gary Hubbard for the computer controlled and data reduction software.

References

1. Chan, C. K., Lau, K. S., Chin, W. K., and Cheng, R. K., *24th International Symposium on Combustion* , The Combustion Institute, Pittsburgh, PA, p. 511-518 (1992).

2. Cheng, R. K., and Shepherd, I. G., *Combustion and Flame,* 85, p. 7 - 26 (1991).

3. Cho, P., Law, C. K., Hertzberg, J. R. and Cheng, R. K.: 21st Symposium (Int'l) on Combustion, p. 1493, The Combustion Institute, 1986.

4. Cheng, R. K.: Combustion Science and Technology, 41, 109 (1984).

5. Beer J. M. and Chigier N. A. *Combustion Aerodynamics*, Applied Science Publications, London, 1972.

6. Gouldin, F. C., Depsky, J. S., and Lee S.-L.: AIAA Journal 23, 1, 95 (1985).

7. ABD Al-Messeeh, W. A., Bradley, D., Gaskell, P. H., and Lau, A. K. C.: 23rd Symposium (Int'l) on Combustion, p. 825, The Combustion Institute, 1990.

8. Kostiuk, L. W., Bray, K. N. C, and Cheng, R. K. *"Combustion and Flame , 92,* 4, p. 377-395 (1993)

9. Bray, K. N. C., Libby, P. A., and Moss J. B. *Combustion. and Flame*, 61, p. 87-102 (1985).

10. Cheng R. K. and Shepherd I. G.: *Combustion Science and Technology, 52*, p. 353 (1986).

11. Bedat, B, and Cheng, R. K. "Experimental Study of Premixed Flames in Intense Isotropic Turbulence" accepted for presentation at the 25th Symposium (Int'l) on Combustion (1994).

12. Gokalp, I., Shepherd, I. G., and Cheng, R. K., "Spectral Behavior of Velocity Fluctuations of Premixed Turbulent Flames," *Combustion and Flame, 71*, p. 313-323 (1988).

13. Shepherd, I. G. and Cheng, R. K., *Combustion Science and Technology*, 59, p. 341-353 (1988).

15. Shepherd, I. G., and Ashurst, Wm. T. : *24th Symposium (Int'l) on Combustion*, p. 485-491, The Combustion Institute 1992.

15. Cheng, R. K., Talbot, L. and Robben, F., *20th Symposium (Int'l) on Combustion*, p. 453 The Combustion Institute, Pittsburgh, PA p.453 (1985).

Table I Experimental Conditions and Flame Speeds for Weak-swirl Flames

Case	Fuel	ϕ	U_∞ (m/s)	Turb. Source	S_L (m/s)	S_F (m/s)	q' (m/s)	q'/S_L	S_F/S_L
SWF1	C_2H_4	0.65	5.0	none	0.347	0.52	0.132	0.35	1.51
SWF2	C_2H_4	0.65	5.0	plate	0.347	1.64	0.350	1.01	4.73
SWF4	CH_4	1.00	5.0	grid	0.433	1.400	0.293	0.68	3.23
SWF5	C_2H_4	0.75	3.0	none	0.449	0.83	0.096	0.21	1.85
SWF6	C_2H_4	0.75	3.0	plate	0.449	1.6	0.320	0.71	3.56
SWF7	C_2H_4	0.70	3.0	plate	0.402	1.57	0.260	0.65	3.91
SWF8	C_2H_4	0.60	3.0	plate	0.292	1.23	0.249	0.85	4.21
SWF9	C_2H_4	0.50	3.0	plate	0.182	1.12	0.206	1.13	6.15
SWF10	CH_4	0.9	3.0	none	0.367	0.72	0.137	0.37	1.96.
SWF11	CH_4	0.6	3.0	none	0.148	0.40	0.125	0.85	2.70
SWF12	CH_4	1.00	3.0	plate	0.433	1.620	0.379	0.88	3.74
SWF13	CH_4	0.90	3.0	plate	0.367	1.500	0.315	0.86	4.09
SWF14	CH_4	0.80	3.0	plate	0.296	1.340	0.290	0.98	4.53
SWF15	CH_4	0.70	3.0	plate	0.225	1.289	0.267	1.19	5.73
SWF16	CH_4	0.60	3.0	plate	0.148	1.092	0.243	1.64	7.38
SWF17	CH_4	1.00	3.0	grid	0.433	1.100	0.188	0.43	2.54
SWF18	CH_4	0.90	3.0	grid	0.367	1.086	0.172	0.47	2.96
SWF19	CH_4	0.80	3.0	grid	0.296	0.974	0.173	0.58	3.29
SWF20	CH_4	0.70	3.0	grid	0.225	0.847	0.166	0.74	3.76
SWF21	CH_4	0.60	3.0	grid	0.148	0.743	0.151	1.02	5.02

Table II Experimental Conditions and Flame Speed for Stagnation Plate Stabilized Flames

Case	Fuel	ϕ	U_∞ (m/s)	Turb. Source	S_L (m/s)	S_F (m/s)	q' (m/s)	q'/S_L	S_f/S_L
S1	CH_4	1.00	5.00	plate	0.433	1.620	0.338	0.78	3.74
S3	CH_4	0.75	5.00	plate	0.260	1.150	0.280	1.08	4.42
S4	CH_4	0.85	5.00	plate	0.333	1.240	0.320	0.96	3.72
S9	C_2H_4	1.00	5.00	plate	0.734	2.69	0.470	0.64	3.66
S10	C_2H_4	0.85	5.00	plate	0.578	2.24	0.424	0.73	3.88
S11	C_2H_4	0.75	5.00	plate	0.449	1.51	0.336	0.75	3.36

Figure Captions

Figure 1 Direct flame luminosity photographs of non-turbulent (a) and turbulent flames (b) stabilized by weak swirl.

Figure 2 Schematics of the burner and diagnostics.

Figure 3 Comparison of the velocity spectra obtained for the longitudinal velocity fluctuations in three turbulent flows.

Figure 4 Two dimensional velocity vectors measured in (a) non-turbulent isothermal swirl flow, (b) non-turbulent flame SWF10, (c) turbulent isotherm swirl flow, (d) turbulent flame SWF18.

Figure 5 Correlation of flame speed with averaged RMS velocity.

Figure 6 Centerline profiles of SWF4.

Figure 7 Normalized profiles of flame crossing frequencies ν.

Figure 8 Normalized relative velocities ΔU for selected cases.

Figure 9 Comparison of centerline and off-center flowline profiles of SWF1.

Figure 10 Comparison of centerline and off-center flowline profiles of SWF4.

Figure 11 Evolution of centerline profiles with equivalence ratio.

Figure 12 Contours of the unconditioned velocity jpdfs obtained at the center of the flame brushes of SWF10 through 15.

Figure 13 Values of K_t determined for selected weak-swirl stabilized and stagnation flow stabilized flames.

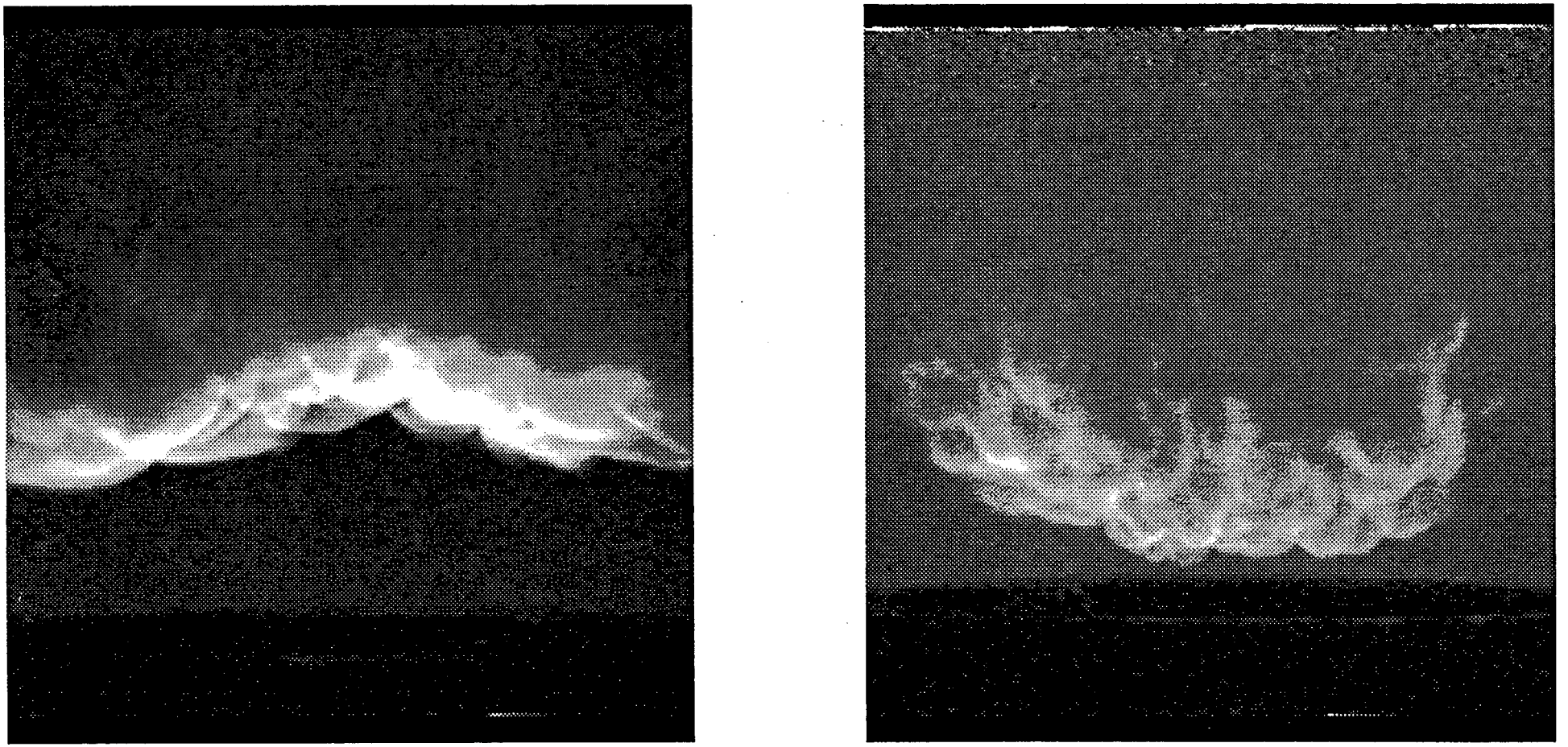

Figure 1 Direct flame luminosity photographs of non-turbulent (left) and turbulent flames (right) stabilized by weak swirl.

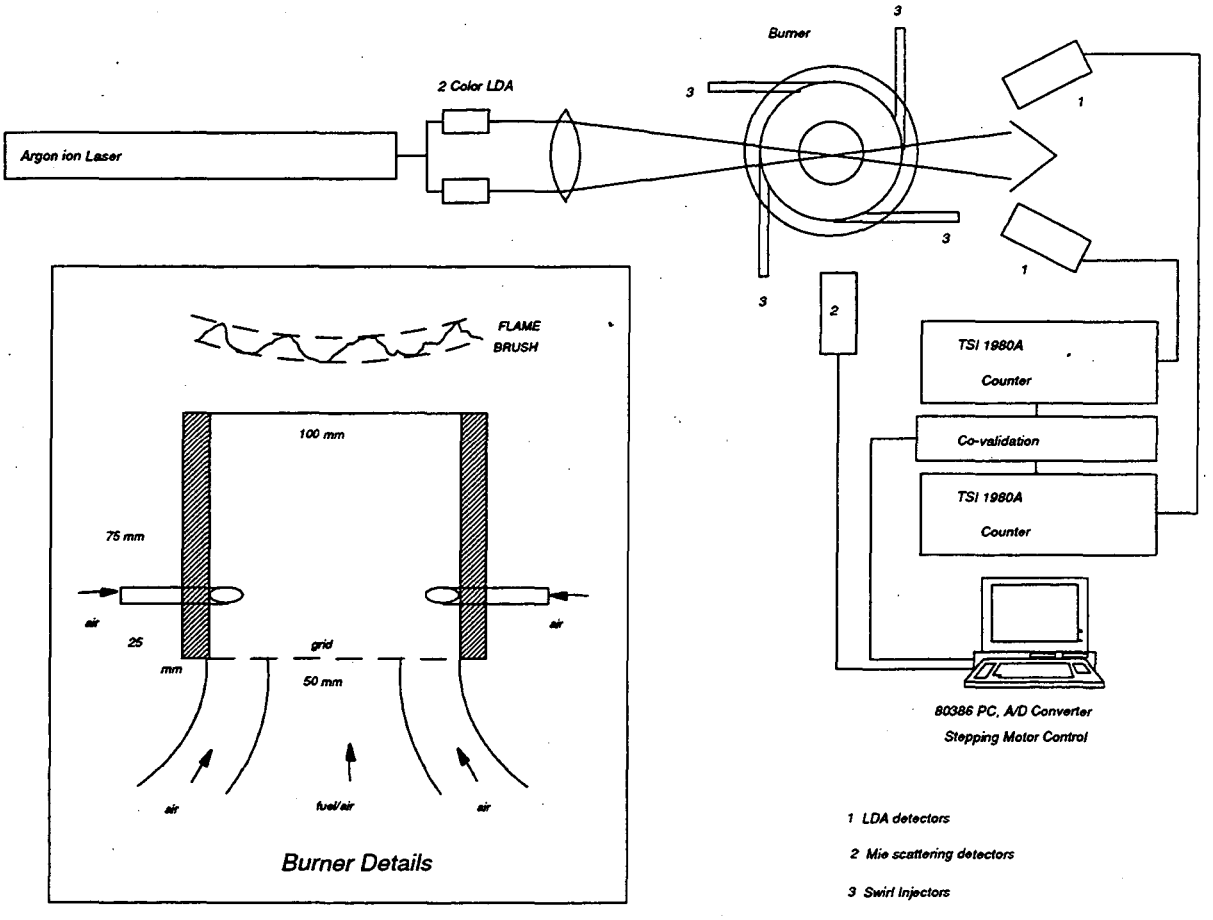

Figure 2 Schematics of the burner and diagnostics

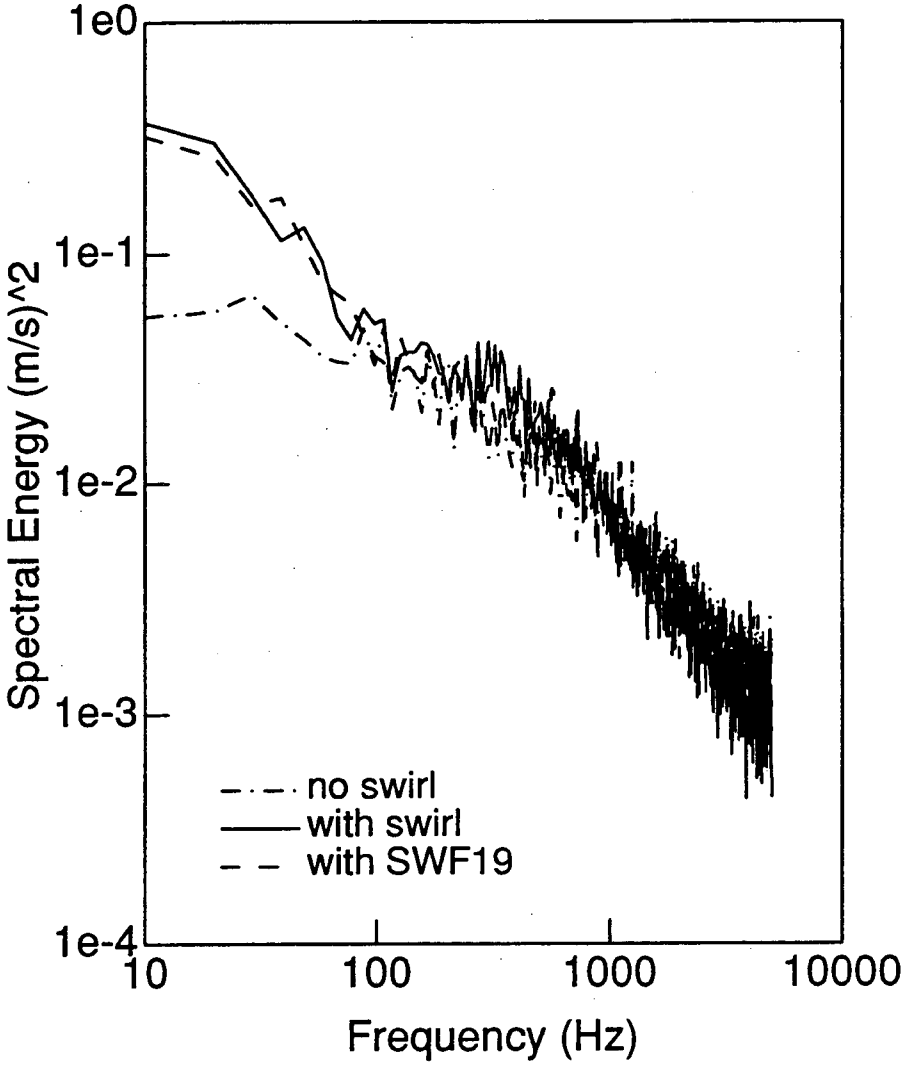

Figure 3 Comparison of the u' spectra

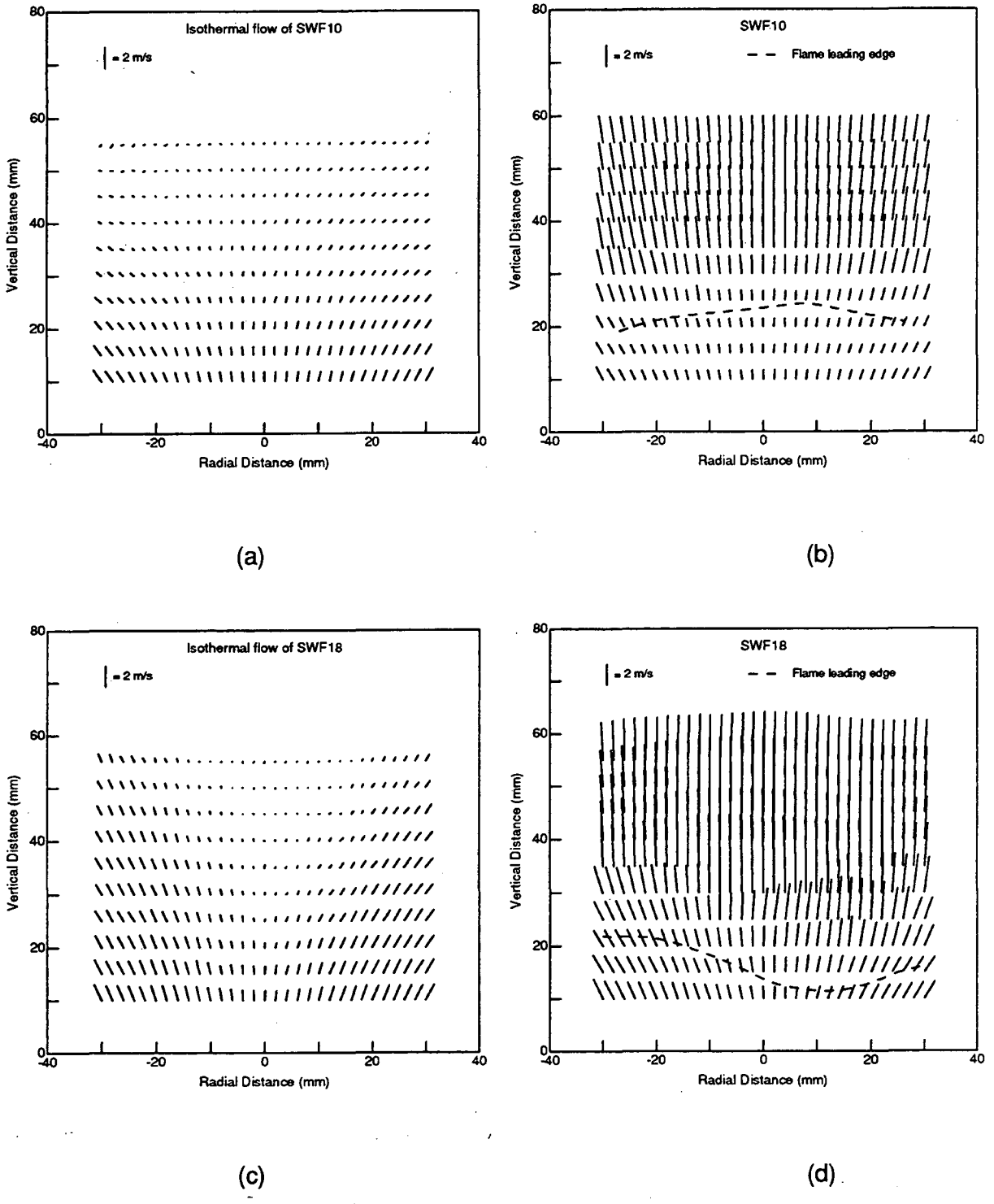

Figure 4 Two dimensional velocity vectors measured in (a) non-turbulent isothermal swirl flow (b) non-turbulent flame SWF10 (c) turbulent isothermal swirl flow, (d) turbulent flame SWF18.

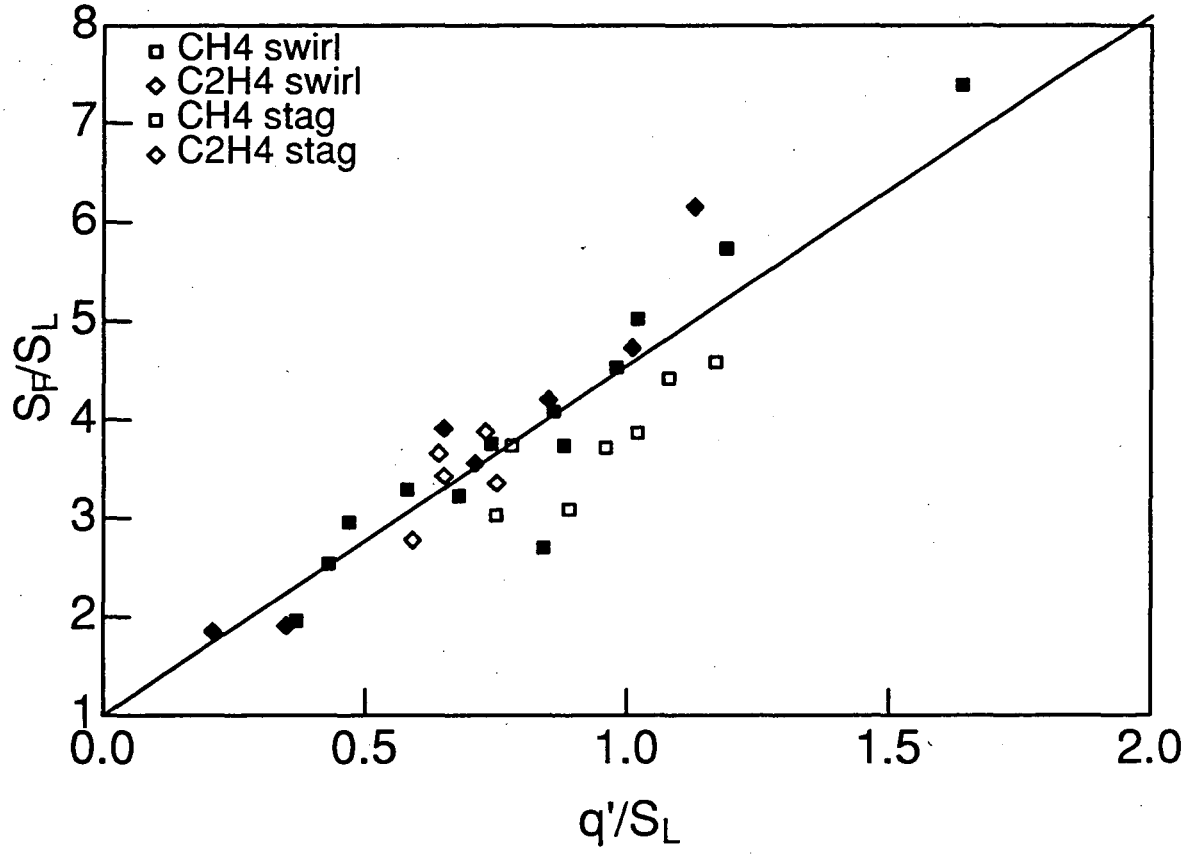

Figure 5 Correlation of flame speed S_F with averaged RMS velocity q'.

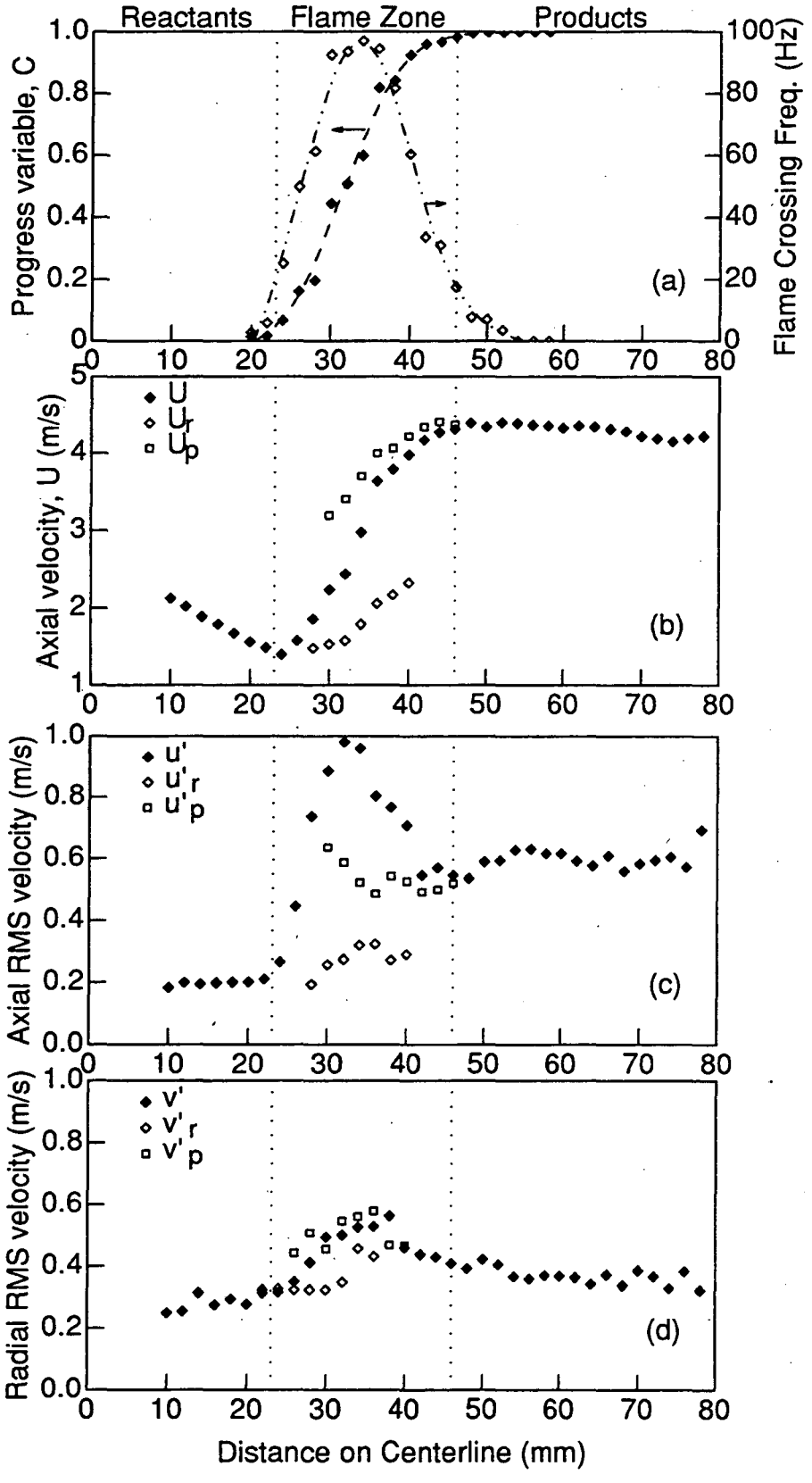

Figure 6 Cenerline profiles of SWF4

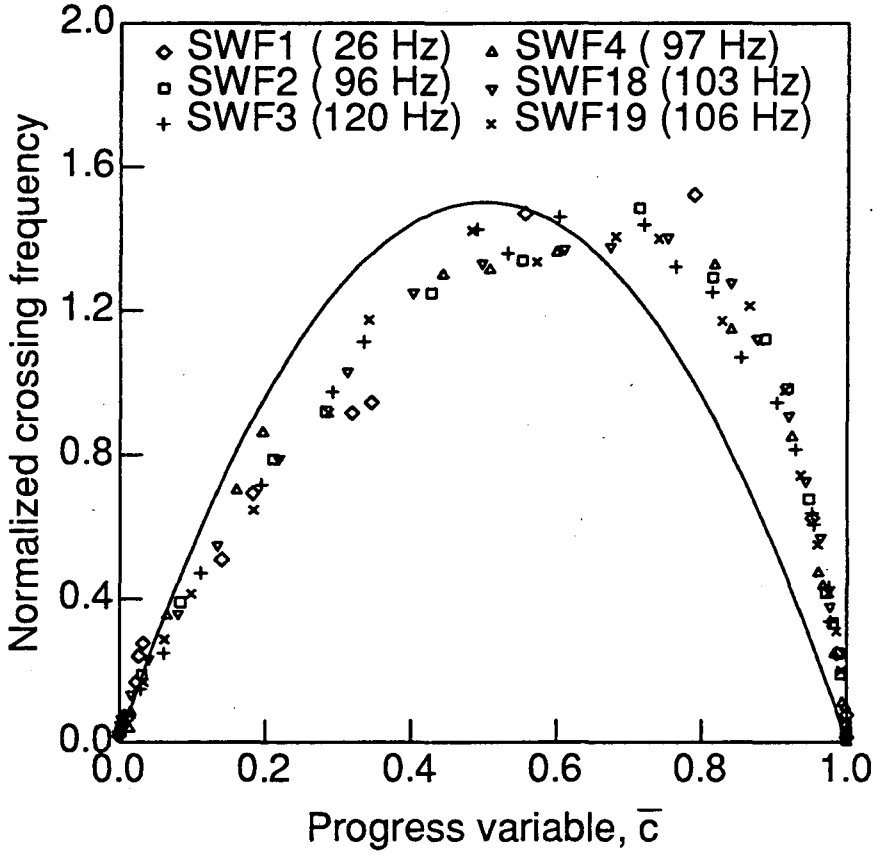

Figure 7 Normalized flame crossing frequencies ν.

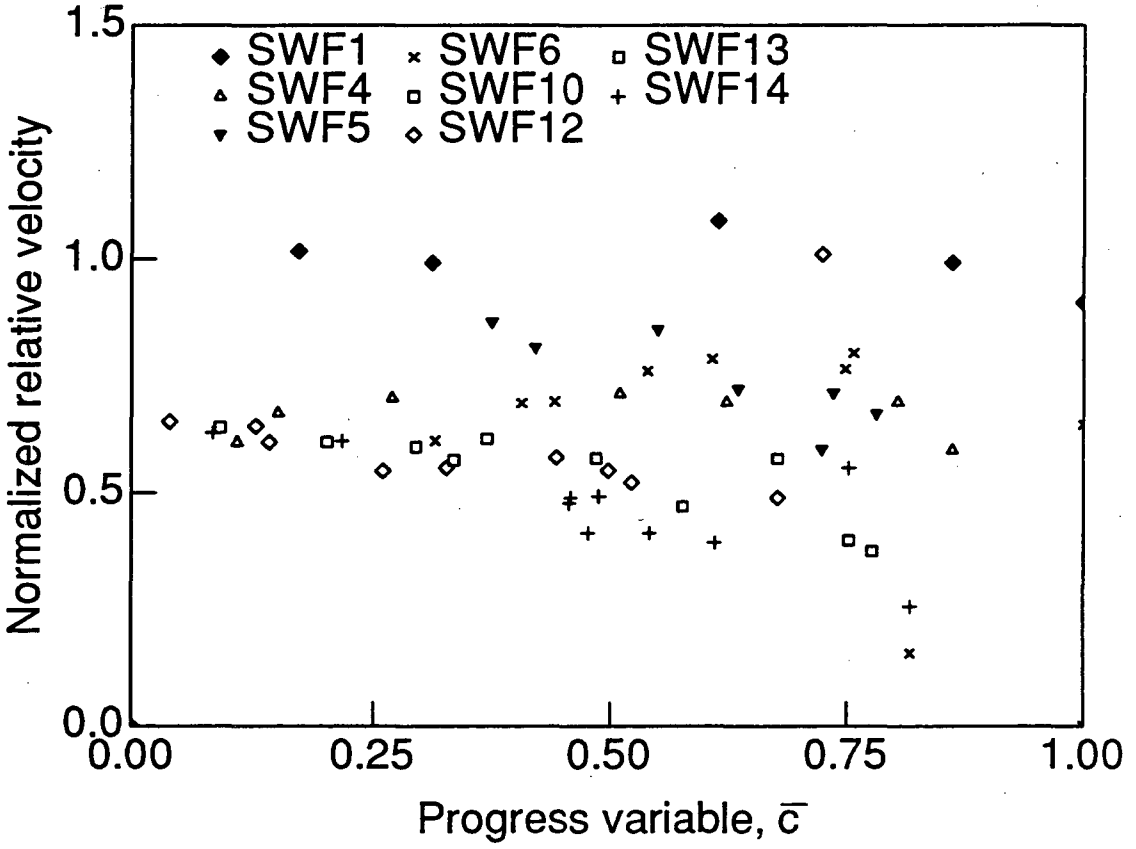

Figure 8 Normalized relative velocity ΔU for selected cases.

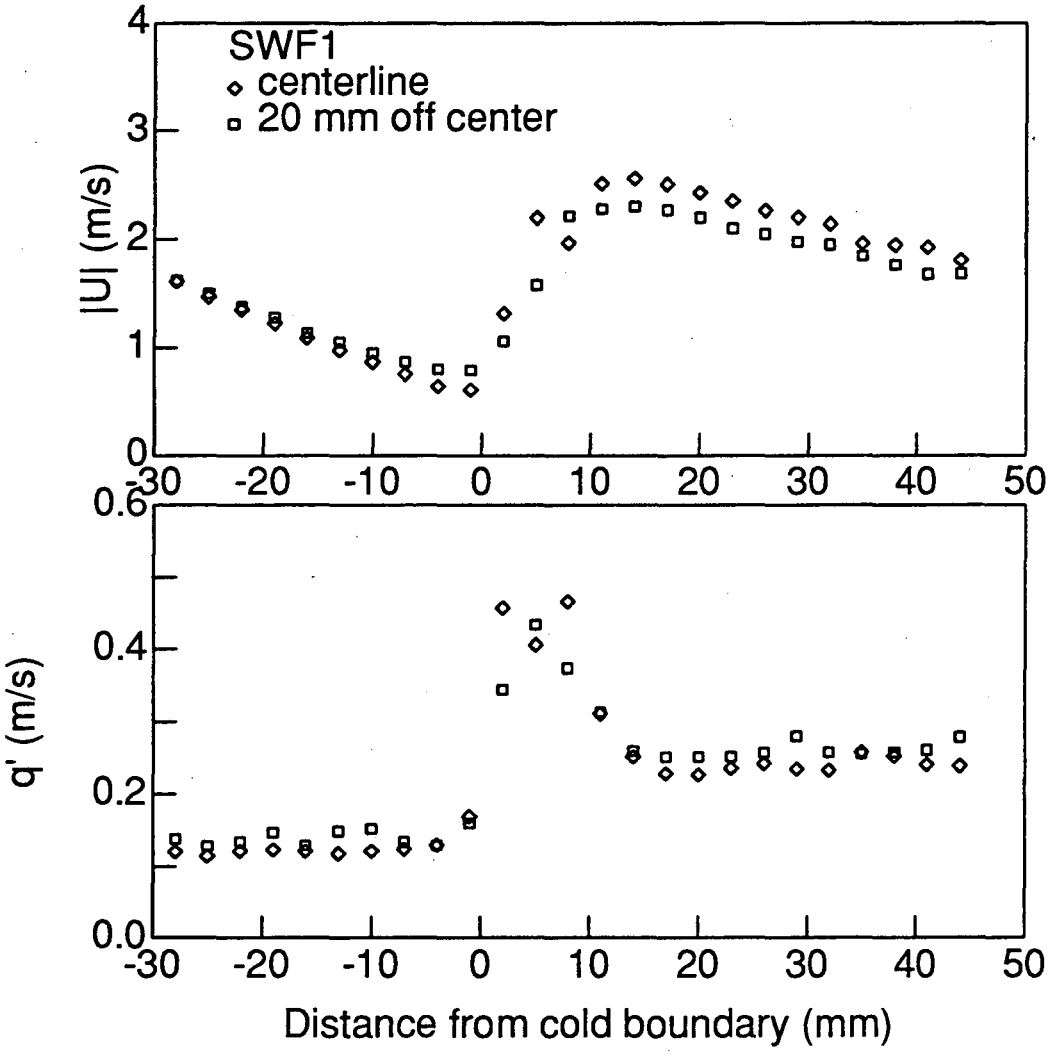

Figure 9 Comparison of the centerline and off-centerline profiles of SWF1.

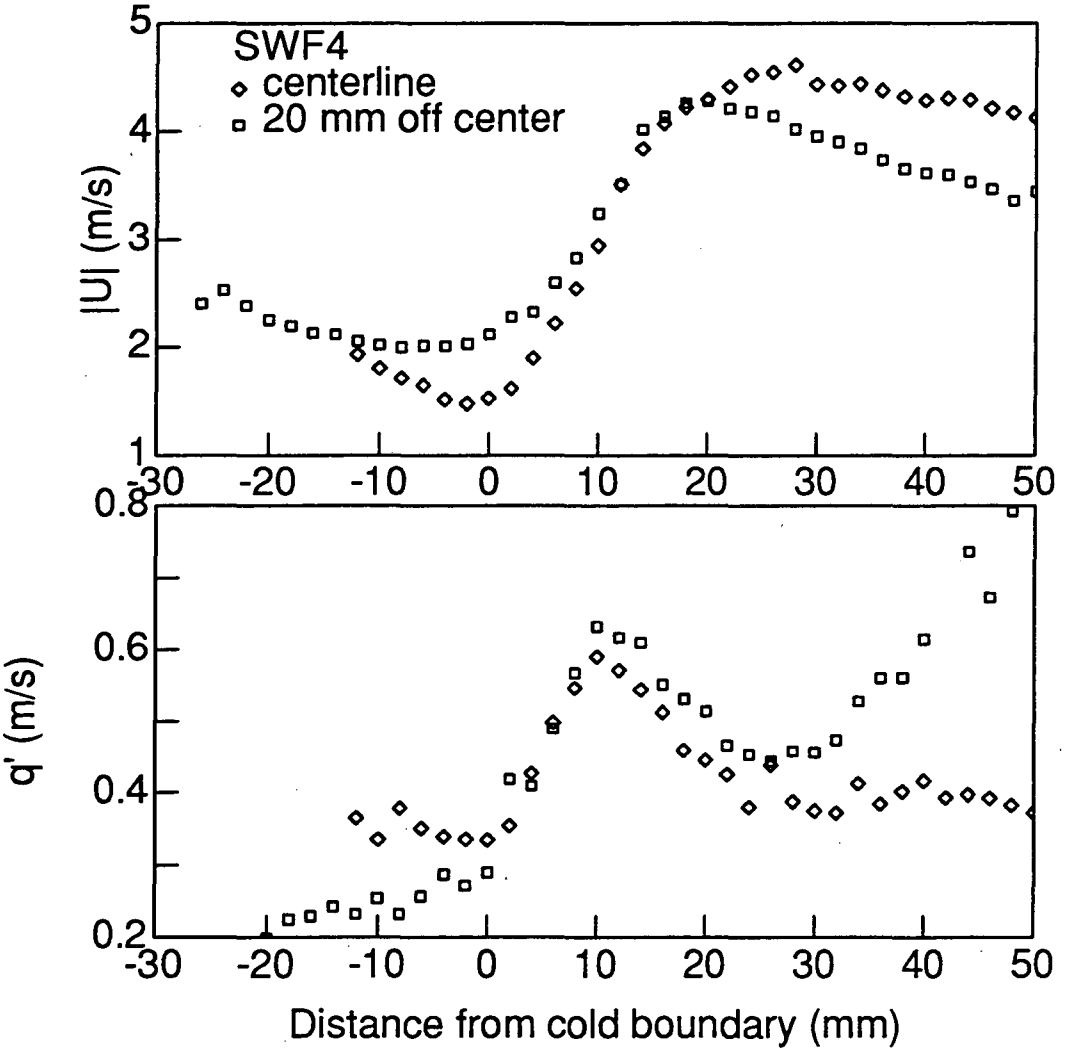

Figure 10 Comparison of the centerline and off-cenerline profiles of SWF4.

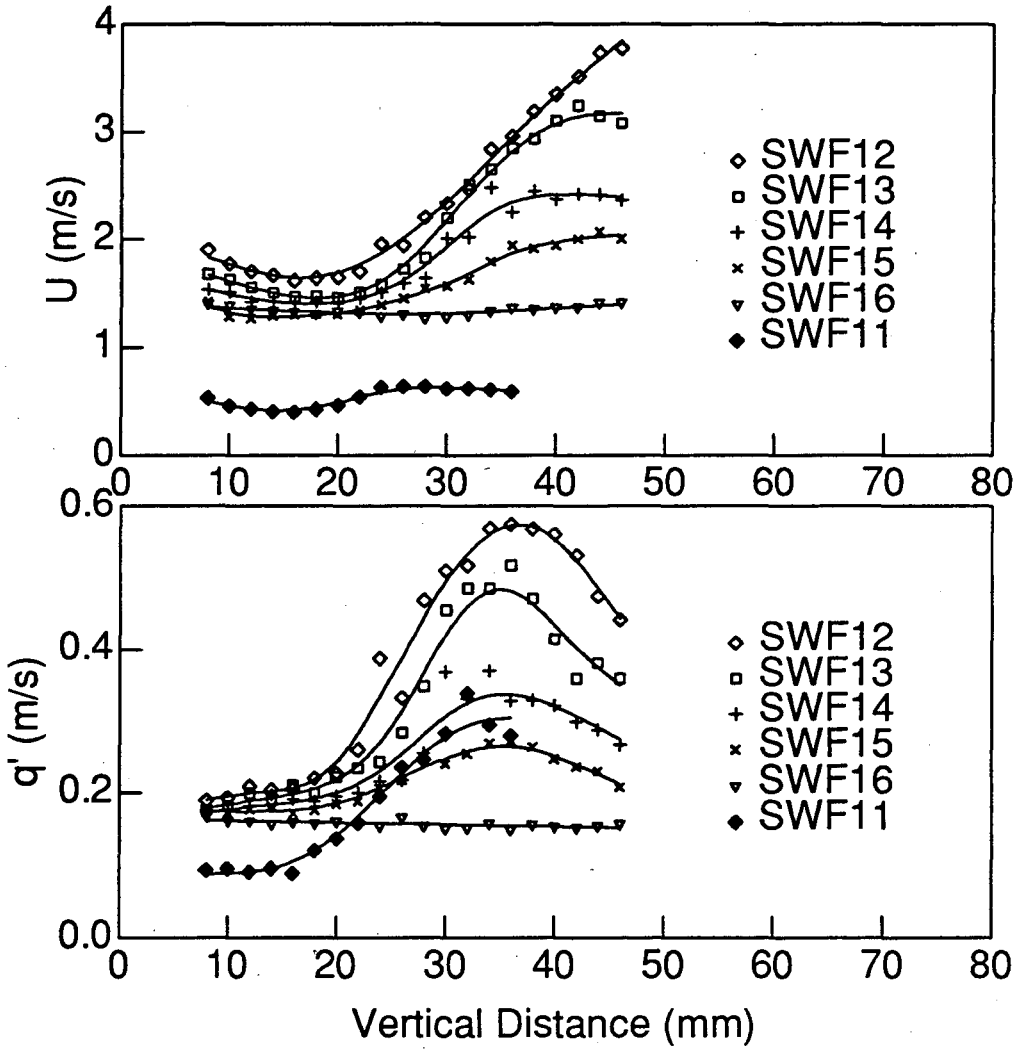

Figure 11 Evolution of the cenreline velocity profiels with ϕ.

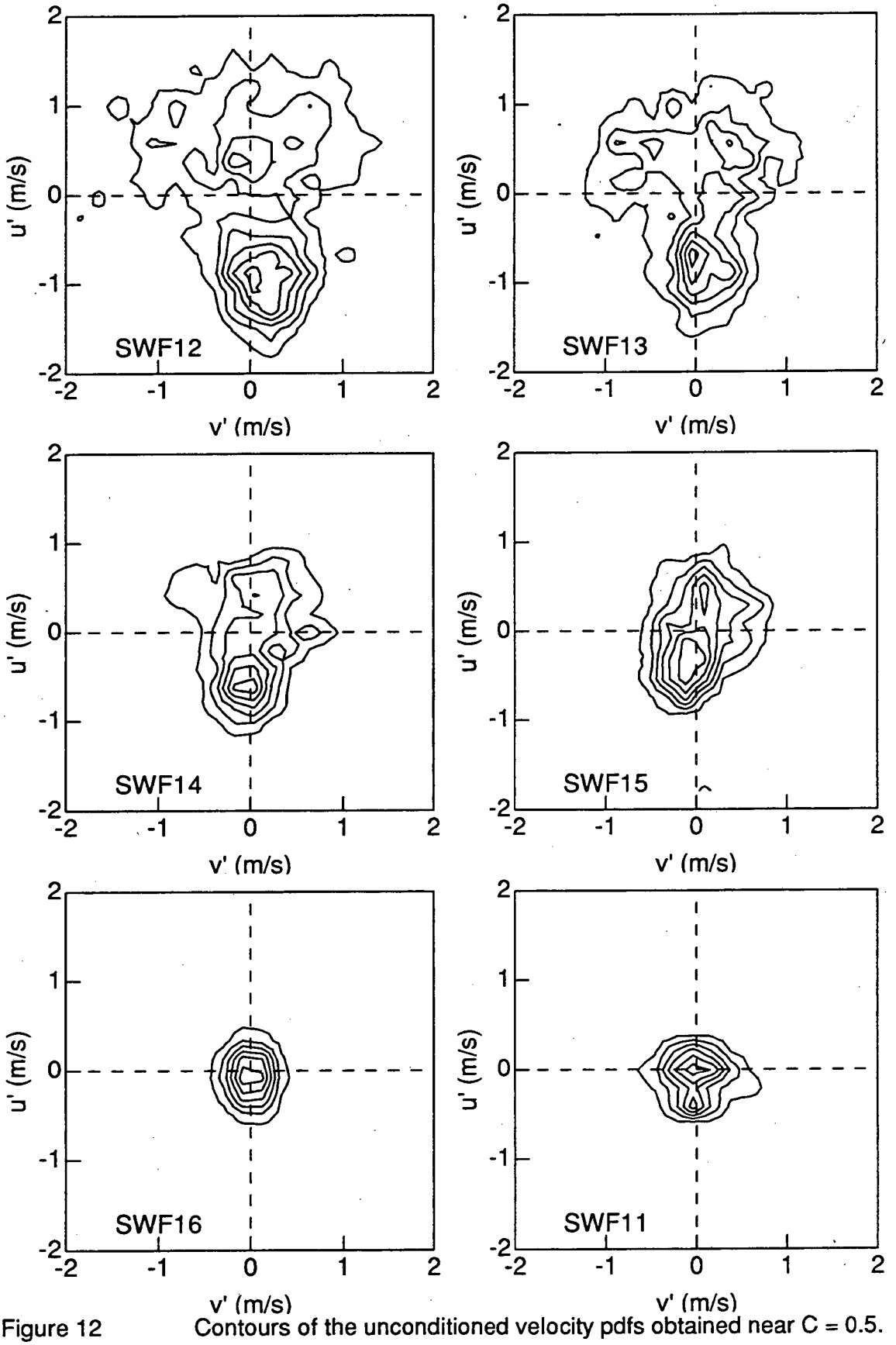

Figure 12 Contours of the unconditioned velocity pdfs obtained near C = 0.5.

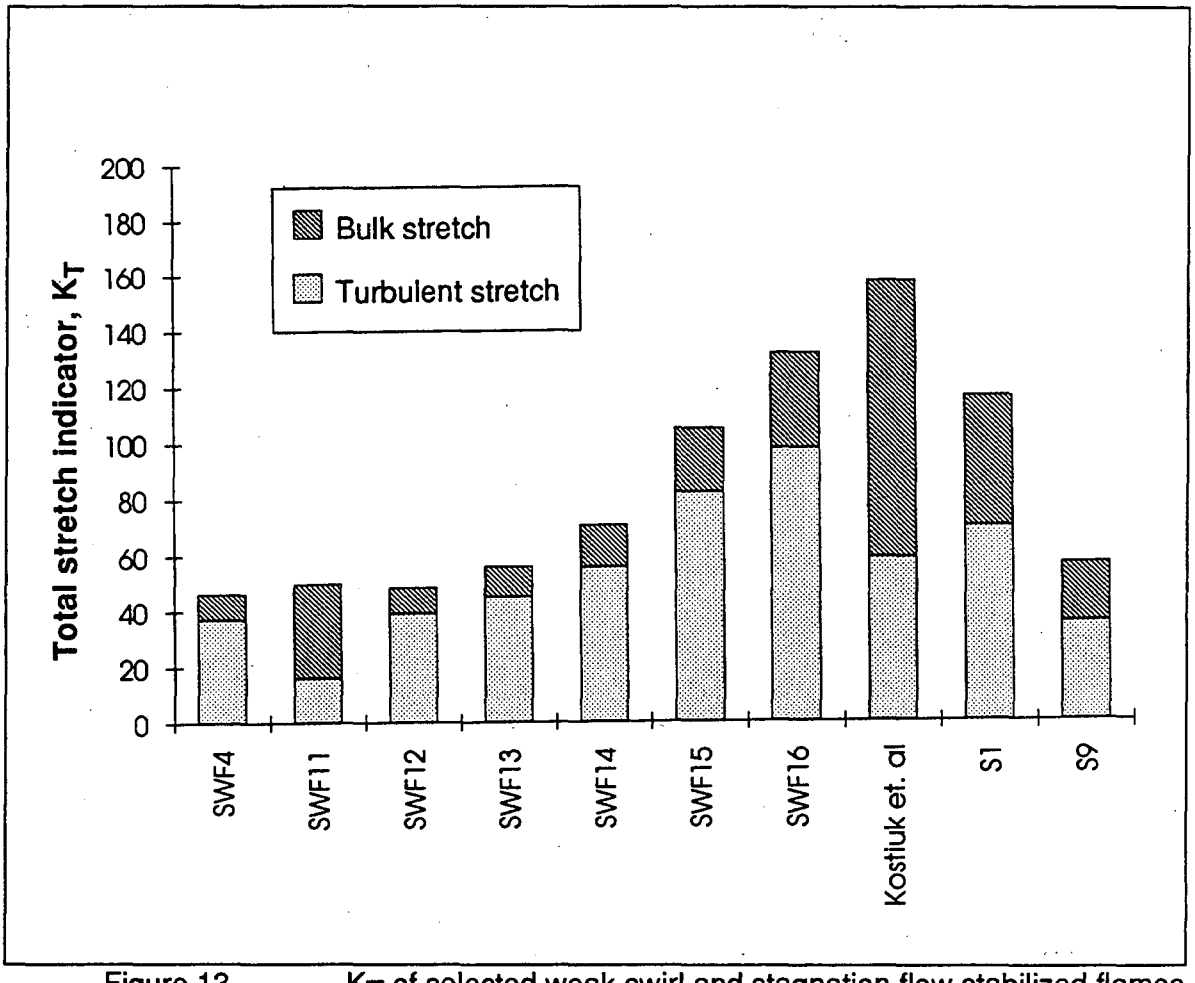

Figure 13 K_T of selected weak-swirl and stagnation flow stabilized flames

LAWRENCE BERKELEY LABORATORY
UNIVERSITY OF CALIFORNIA
TECHNICAL INFORMATION DEPARTMENT
BERKELEY, CALIFORNIA 94720